Design And Fabrication Of Thin-Film Optical Filters For Mid-Infrared Spectroscopy Application

Ayman Zohbi, M.A. Hasan

Abstract: This paper reports the design, fabrication, and results of thin film Fabry-Perot interferometer (FPI) for mid-infrared spectroscopy application. The system is designed to be integrated in a small portable spectrometer for the measurement of molecular absorption or emission as well as substance that has an infrared signature. The filter is based on Fabry-Perot interferometer and the wavelength of interest is in the mid-infrared (5 to 15 micrometers). The layers were selected carefully to minimize the thickness required to meet the quarter-wave optical-thickness criteria for the interferometer.

.

Index Terms: Fabry-Perot filter, finesse, Infrared filter, interferometer, spectroscopy, Bragg reflector.

1 INTRODUCTION

Spectroscopy has been used in many fields and industries for a variety of measurements. For instance it is used to monitor certain gas species for environmental and industrial measurements, as well as to measure the consistency of chemical coating. In the medical field it is used for a variety of applications ranging from tissue oxygen measurement to the detection of toxic molecules and drugs. It is even used by law enforcement for the detection of explosives and hazardous material [10]-[13]. A traditional spectrometer consists of a complex system of optical lenses and moving mirrors and it is, therefore, bulky and expensive. By using conventional VLSI fabrication techniques a small, portable spectrometer can be produced with considerably reduced cost. A portable spectrometer will offer the flexibility of making measurement quickly and anywhere without the need to expensive laboratory analysis. Depending on the application, such a system can be designed as an array based spectrometer with each cavity pre-tuned to a specific wavelength or as MEMS based spectrometer that can be tuned by varying the gap in the cavity with an electrical potential.

2 FABRY-PEROT FILTER DESIGN

A typical Fabry-Perot interferometer and its transmission are illustrated in Figure 1(a) and 1(b) respectively. Assuming M1 and M2 are two mirrors perfectly parallel to each other, then the light waves in the cavity reflect back and forth between M1 and M2. Those light waves interfere constructively and destructively resulting in standing EM waves [1].

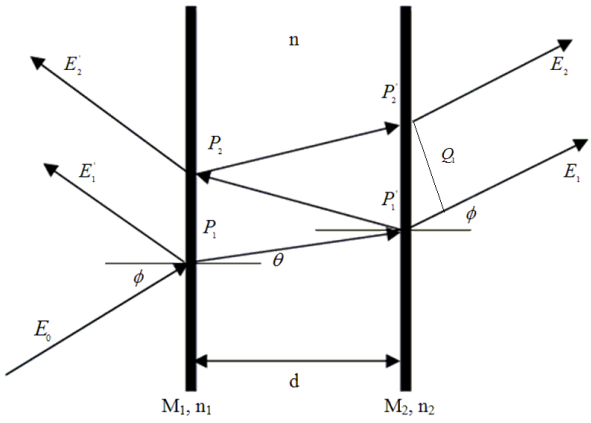

(a)

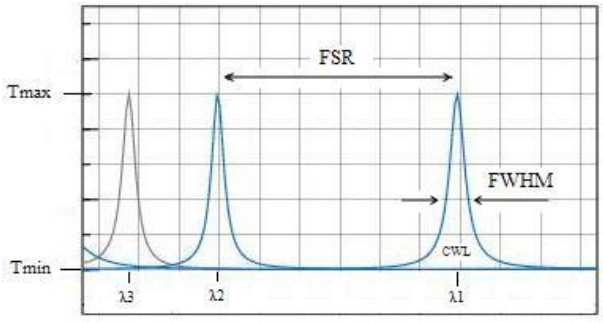

(b)

Figure 1: (a) Schematic of an FPI. *M1* and *M2* are the two mirrors; d is the distance between the mirrors; ϕ is the angle of incident light, and θ is the phase shift at reflection. (b) Transmission spectrum of an FPI. The transmittance spectrum of a FPI is illustrated in figure 1 (b) and described by the airy-function in equation (1). Assuming the two reflectors have the same reflectance R and the same absorbance A, the transmission T can be described as follows [2]:

$$T = \left(1 - \frac{A}{(1-R)}\right)^2 \frac{1}{1 + \left(\frac{4R}{(1-R)^2}\right)\sin^2\left(2\pi n d \frac{1}{\lambda}\cos\theta - \phi\right)} \qquad (1)$$

- *Ayman Zohbi, University of North Carolina at Charlotte, ECE department.*
- *M.-A. Hasan, University of North Carolina at Charlotte, ECE department.*

To simplify the discussion, we assume that the angle of incidence is zero and the phase change on reflections is π, then equation (1) becomes:

$$T = \left(1 - \frac{A}{(1-R)}\right)^2 \frac{1}{1 + \left(\frac{4R}{(1-R)^2}\right)\sin^2\left(\frac{2\pi nd}{\lambda}\right)}$$

The transmission peaks occur when the following condition is satisfied:

$$\frac{2\pi nd}{\lambda} = m\pi \Rightarrow \lambda_m = \frac{2nd}{m} \qquad (2)$$

where n is the refractive index of the cavity and m is an integer that corresponds to the cavity mode. The spectral resolution of a FPI, which determines the spectral bandwidth (FWHM), is described in equation (3) [2].

$$FWHM = \frac{1}{2d\pi}\frac{1-R}{\pi\sqrt{R}} \qquad (3)$$

The spectral distance between two adjacent peaks or resonant wavelengths is called the Free Spectral Range (FSR), and the ratio of FSR and FWHM is called the Finesse and it is described in equation (4) [2]:

$$\tilde{F} = \frac{FSR}{FWHM} = \frac{\pi\sqrt{R}}{1-R} \qquad (4)$$

The performance of a Fabry-Perot interferometer depends on the reflectivity of the mirrors. The higher the reflectance (R) the sharper and narrower the transmission peaks of the filter. Therefore, as R increases FWHM decreases. There are two commonly used materials in the fabrication of optical mirrors, metal thin film, and multilayer dielectric coatings. However, dielectric mirrors are characterized by their robustness, low maintenance, and low absorption loss [3].

2.1 Dielectric Mirrors

Dielectric mirrors consist of stacking alternating layers of dielectric materials of low and high reflective indices. The high reflectance is achieved due to the fact that when the light beams reflect at the interfaces of the different layers, they all reach the front surface having the same phase shift, which allows them to interfer constructively. This stack of dielectric layers is also called Distributed Bragg Reflector. For a given wavelength, the reflectance in air for this stack of layer is given by equation (5)[3]:

$$R = \left(\frac{1 - (n_H/n_L)^{2p}(n_H^2/n_S)}{1 + (n_H/n_L)^{2p}(n_H^2/n_S)}\right)^2 \qquad (5)$$

Where n_H, n_L, and n_S are the indices of refractive of the high index, low index and the substrate layers respectively, p is the pairs of high/low-index layers. The relationship between reflectivity and the number of stack layers is depicted in figure (2) below.

Figure 2: Reflectance with different number of stack layers. As depicted in the figure 2, the higher the stack layers, the higher

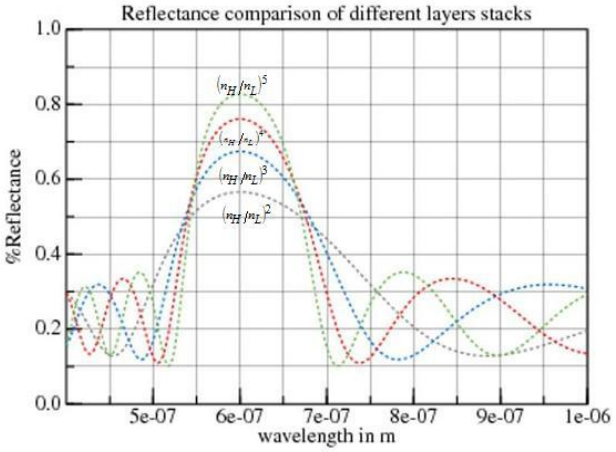

the reflectivity of the dielectric mirrors, and this results in a sharper and narrower peak.

2.2 Filter Design

The Fabry-Perot filter was designed for central wavelength of 9.2 µm, with the ability to be tuned at 8.4 µm and 10.1 µm. The dielectric mirros design is based on the Bragg reflector structure which consists of alternating quarter wave optical thickness (QWOT) layers with low and high refractive index. In order to build high reflective mirrors in the desired wavelength range, without stacking too many layers of thin films, the refractive index ratio n_H/n_L has to be as high as possible. Potential thin films to be used as a low refractive index material are zinc oxide (ZnO) or zinc sulfide (ZnS) and germanium (Ge) as high refractive index material. The refractive index n of Ge, ZnS, and ZnO are shown in figures 3 below [4].

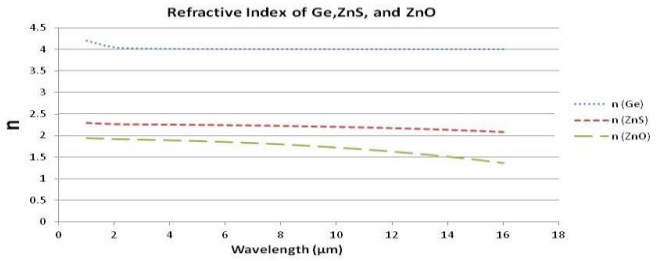

Figure 3: Refractive index of Germanium (Ge), Zinc Sulfide (ZnS), and Zinc Oxide (ZnO).

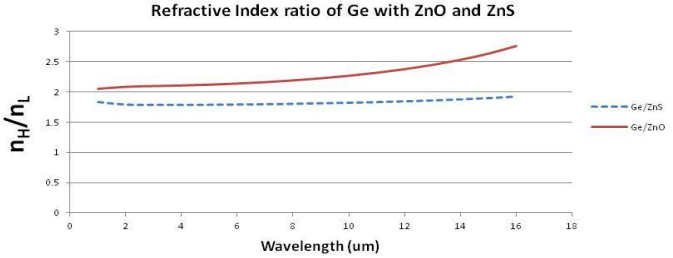

Figure 4: Refractive index ratio of Ge/ZnO and Ge/ZnS

Based on the plot of figure 4, the Ge/ZnO ration will give us higher reflectivity than the Ge/ZnS ratio. The ZnO layer is deposited by sputtering process and the Ge layer was deposited by the e-beam process. The layers thicknesses (d) was calculated according to the quarter wave optical thickness method:

$$d = \frac{\lambda_c}{4n}$$

Where λ is the center wavelength, *n* is the refractive index of the material, and *d* is the layer thickness. Table 1 below summarises the design parameters of the filter. Where m is the order number, λ_m is the center wavelength, and d is the distance between mirrors.

Table 1: FPI design parameters

λ_c	8.4	9.2	10.1
λ/m	8.4	9.2	10.1
Design Parameters (m=1)			
Value	d/m	d (um)	
1	4.2	4.2	
2	4.5	4.5	
3	5.05	5.05	

2.3 Mechanical Design

The Fabry-Perot interferometer is designed with two fixed mirrors separated by a distance d. Each mirror consists of a stack of alternating layers of dielectric materials, Ge as a high index material, and ZnO as a low index material. The layers are deposited on a 300 µm thick silicon substrate as illustrated in figure 5 below.

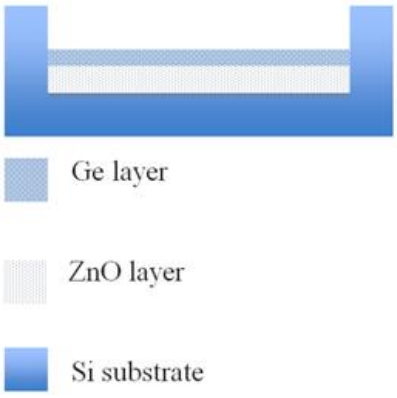

Figure 5: Mirror structure

The silicon wafer must be cleaned of any contamination at all the fabrication stages. The wafer was first cleaned in a 2-3 solution of Hydrogen Peroxide (H_2O_2) and Sulfuric acid (H_2SO_4) to remove any organic and metallic materials. After that the wafer was rinsed in de-ionized (DI) water for 5 minutes. Then the wafer was dipped in a 10% Hydrofluoric Acid (HF) for 10 seconds, to remove any oxide impurities from the wafer.

The fabrication process is depicted in the following steps:

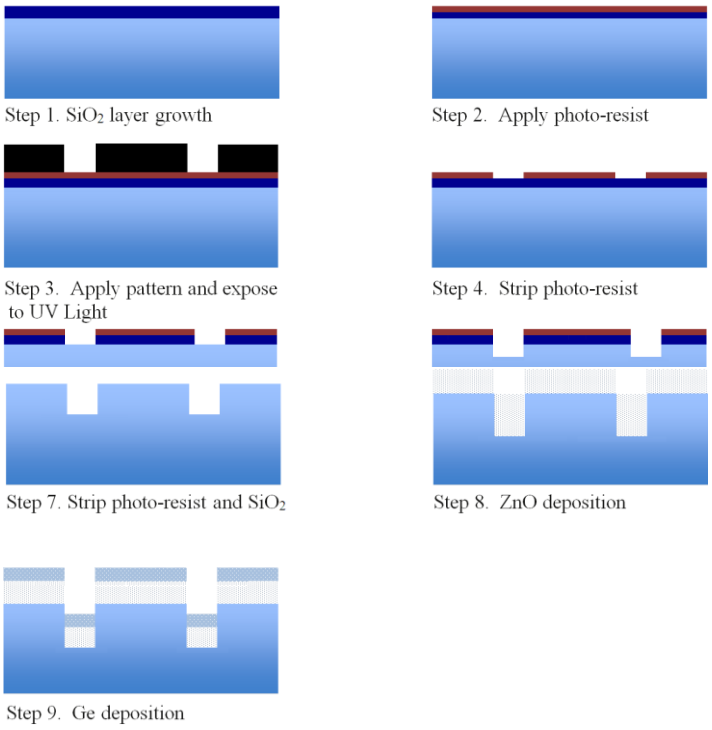

Step 1. Oxidation Process

A dry and wet oxidation processes used to grow the SiO_2 layer on the silicon wafer as follows:

1- $Si + N_2 + O_2 \longrightarrow SiO_2 + N_2$ (5 minutes, dry)

2- $Si + N2 + 2H_2 + 2O_2 \longrightarrow SiO_2 + 2H_2O + N_2$ (40 minutes, wet)

3- $Si + N_2 + O_2 \longrightarrow SiO_2 + N_2$ (5 minutes, dry)

Step 2. Apply Photoresist

A blob of positive photoresist (Microposit 1813) is applied on the wafer and then spun for 60 seconds at 4000 rpm, to give an evenly spread layer of photoresist. The wafer is then soft-baked on a hot plate (115 C) for 60 seconds, which allows for better adhesion of the photoresist to the silicon wafer.

Step 3. Apply pattern and expose to UV Light

Align the mask/pattern on the silicon wafer, then expose to Ultra-Violet (UV) light for 40 seconds. This process allows the exposed photoresist to develop in the photoresist developer.

Step 4. Strip photo-resist

After exposure to UV light, submerse the silicon wafer in the photoresist developer solution to wash away the exposed photoresist and copy the mask pattern to the silicon wafer.

Step 5. Remove the SiO_2

To remove the SiO_2 layer, the wafer was submersed in a 10% HF for 20 seconds, then rinsed in DI water for 10 seconds.

Step 6. Etch of Si wafer

The silicon was etched in a 45% Potassium hydroxide (KOH) at 70 C for 3 to 5 minutes to get the required etch thickness.

Step 7. Strip photo-resist and SiO_2

After etching the Si it was time to remove the photoresist and the SiO_2.The photoresist was stripped by submersing the wafer in Acetone for 5 minutes, then Methanol for 5 minutes, and finally rinsing in DI water for 5 minutes and then drying with nitrogen.

The SiO_2 was removed by submersing the wafer in 10% HF for 20 seconds, rinsing in DI water for 10 minutes and then drying with nitrogen.

Step 8. ZnO deposition

The ZnO film was deposited using sputtering deposition technique . Sputtering technique is a process by which the Si wafer (or any substrate where the film will be grown) is placed in a vacuum chamber filled with Argon gas. Then a high voltage is applied in the chamber to ionize the gas and create plasma. The Ar^+ ion accelerates towards the target at high speed and knock off atoms from its surface. These atoms hit the substrate and condense as a film.

Step 9. Ge deposition

The Ge thin film was deposited by the E-beam deposition technique. The e-beam or electron beam evaporation process is an evaporation deposition technique where the substarte is placed in a vacuum chamber and the material to be deposited is a placed in graphite crucible. Inside the chamber there is a tungsten filament that is heated and when it gets too hot it starts emiting electrons. These electrons are deflected and focused on the material to be evaporated. Upon hitting the material, the electrons heat it up and cause it to evaporate and deposit on the substrate.

3 TEST MEASUREMENTS

3.1 Layers thicknesses

The layers thicknesses were measured using a Scanning Electron Microscope (SEM) to determine the exact thickness of the ZnO and the Ge layers.

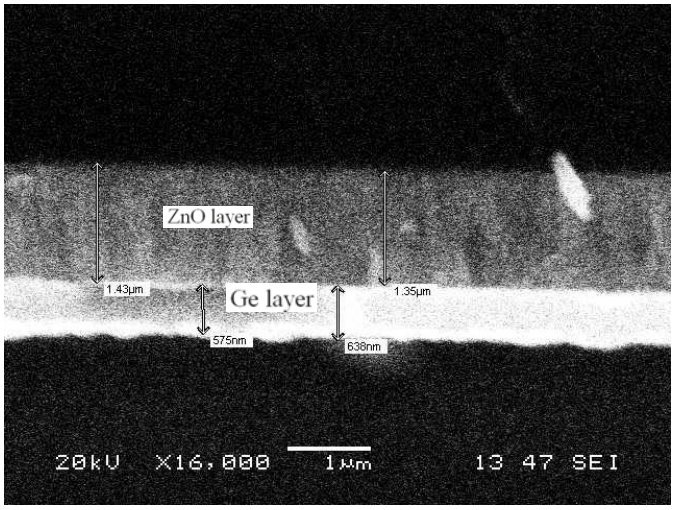

Figure 7: The thicknesses of ZnO and Ge layers measured by SEM.

Based on figure 7, the layers were not uniformly grown, in the case of ZnO the thickness was within 200 nm of the calculated value and the Ge layer within 60 nm of the calculated value.

The fabricated FP filter is tested using Fourier-Transform Infra-Red Spectroscopy (FTIR), and the result then compared with the simulated data.

3.2 Simulation and Measured Results

The simulation was performed using FreeSnell software. Figure 8 below presents the simulated results of FPI design with varying gap distances between the mirrors.

And figure9 presents the actual results of FPI design with varying gap distances between the mirrors.

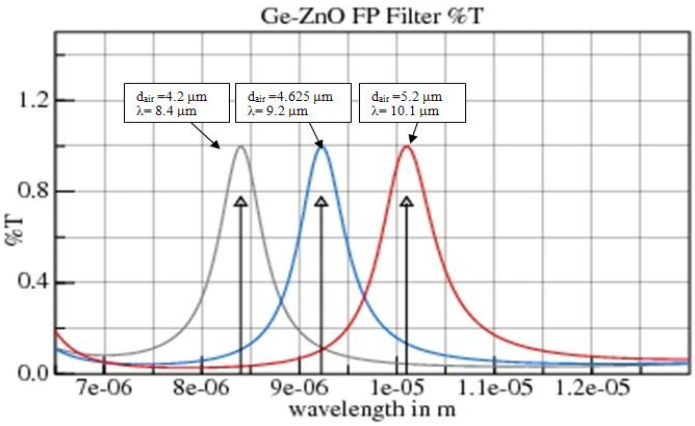

Figure 8: Simulated FP filter with all three different distances d_{air} between the mirrors. The corresponding resonant wavelength of each distance is plotted as well.

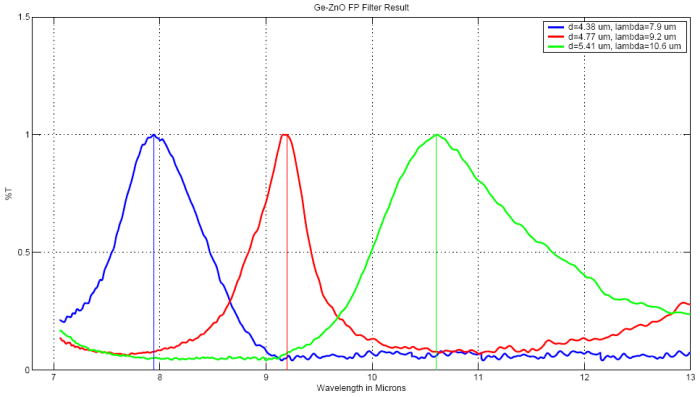

Figure 9: Designed FP filter with all three different distances d_{air} between the mirrors. The corresponding resonant wavelength of each distance is plotted as well.

Table 2 below compares the results obtained from simulation and from the final fabry-perot filter design.

Table 2.
Comparison of the simulation and the final design results

	Design and Simulation comparison					
	FP1		FP2		FP3	
	Simulation	Design	Simulation	Design	Simulation	Design
d_{air}	4.2 mm	4.38 mm	4.6 mm	4.77 mm	5.2 mm	5.41 mm
λc	8.4 mm	7.9 mm	9.2 mm	9.2 mm	10.1 mm	10.6 mm

4 Result Analysis

There is some differences between the simulated and the measured results and that's because the overall performance of the FPI depends on the finesse $\tilde{F}$ of the filter. The finesse determines the bandpass and the sharpness of the transmitted peak. A high finesse filter results in sharp narrow peaks. However flatness, roughness, and smoothness of the mirror surface affect the optical property of the FPI filter. The simulation assumes ideal, flat, and smooth mirrors, perfection that is,practically, hard to achieve. In reality, fabrication imperfections cause deformation of the mirrors surfaces that leads to scattering and consequently reduced reflectivity and finesse [5,6]. Figure 10 illustrates the transmission of an ideal FPI where is figure 11 illustartes the transmission of a non-ideal FPI due to mirors roughness. The figures below illustrate the effect of roughness on the transmitted peaks.

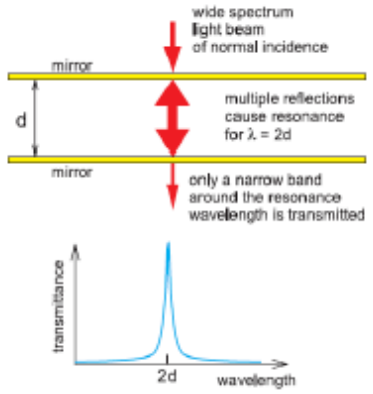

Figure 10: Transmission of an ideal Fabry-Perot interferometer [5].

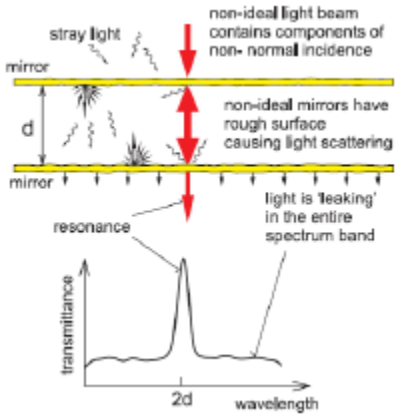

Figure 11: Transmission of a non-ideal Fabry-Perot interferometer [5].

Three types of defects could be introduced during the fabrication process, surface roughness δ_{RMS}, surface spherical deviation from plane δ_S, and plate deviation from parallelism δ_P [6],[7]. If all three types of defects are considered, then the overall finesse defect F_D for a particular wavelength is given by equation (7) [6],[7].

$$\frac{1}{F_D^2} = \left(\frac{2\delta_s}{\lambda}\right)^2 + \left(\frac{4.7\delta_G}{\lambda}\right)^2 + \left(\frac{\sqrt{3}\delta_P}{\lambda}\right)^2$$

$$F_D = \frac{\lambda}{\sqrt{[4\delta_S^2 + 22.09\delta_{rms}^2 + 3\delta_P^2]}} \quad (7)$$

And the effective finesse is given by:

$$F_E = \frac{1}{\sqrt{(1/F_R^2)+(1/F_D^2)}}$$

The impact of mirrors defects on the finesse and thus the sharpness of the transmission peaks is depicted in figure 12 below which shows that higher reflectance results in a sharper transmition peak.

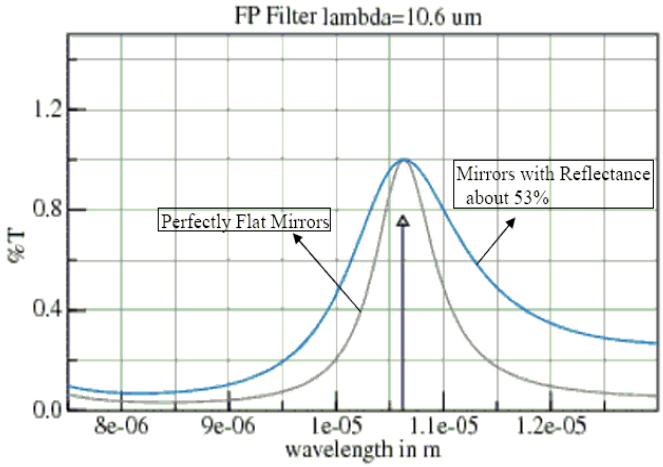

Figure 12: A comparaison between the result of FP with perfectly flat mirrors and non-ideal mirrors that result in reflectance of 53%.

The actual spectrum of the 10.6 μm wavelength is more related to a reflectance of approximately 53% which corresponds to a finesse of 4.86. The reduced finesse is mainly due to the surface roughness which could have been accured during the fabrication process specially during the Si etching process [8],[9].

References

[1] S.O. Kasap "Optoelectronics and Photonics: Principles and Practices" 294-2001.

[2] N. Neumann, M. Ebermann,. Kurth, K. Hiller, S, "Tunable infrared detector with integrated micromachined Fabry-Perot filter", J.Micro/Nanolith. MEMS MOEMS 7(2), 021004-01 - 021004-9 (2008).

[3] H. A. Macleod, "Thin Film Optical Filters", 3rd Edition, Institute of Physics, London, 2001.

[4] http://refractiveindex.info/

[5] M. Bartek, I. Novotný, J.H. Correia, V. Tvarožek "Quality Factor of Thin-Film Fabry-Perot Resonators: Dependence

on Interface Roughness".

[6] E.Jesper Eklund and Andrei M. Shkel. "Performance Tradeoffs in MEMS Sensors with High-Finesse Fabry-Perot Interferometry Detection".

[7] G. A. Gary, E. A. West, D. Rees, J. A. McKay, M. Zukic, and P. Herman, "Solar CIV vacuum-ultraviolet Fabry-Perot interferometers"

[8] E. D. Palik, O. J. Glembocki, I. Heard, P. S. Burno, and L. Tenerz, "Etching roughness for (100) silicon surfaces in aqueous KOH", J. Appl. Phys. 70, 3291 (1991); doi: 10.1063/1.349263.

[9] Gregory t. a. Kovacs, Nadim i. Maluf, and Kurt e. Petersen, "Bulk Micromachining of Silicon".

[10] Frank K. Tittel, Dirk Richter, and Alan Fried "Mid-Infrared Laser Applications in Spectroscopy"

[11] Thomas Muehlemann, Daniel Haensse, Martin Wolf, "Wireless miniaturized in-vivo near infrared imaging", 2008 Optical Society of America.

[12] Hilde A. Rinia, Mischa Bonn, Erik M. Vartiainen,Chris B. Schaffer, and Michiel Müllera, "Spectroscopic analysis of the oxygenation state of hemoglobin using coherent anti-Stokes Raman scattering".

[13] Cynthia L. O'Malley, and Derrick Castle, "FOURIER TRANSFORM INFRARED SPECTROSCOPY TO VERIFY CHEMICAL CONSISTENCY OF INDUSTRIAL COATINGS".